BLUNT-BODY FLOW SIMULATIONS WITH ADVANCED EDDY-VISCOSITY AND REYNOLDS-STRESS TURBULENCE CLOSURES

Enda Dimitri Vieira Bigarella
Instituto Tecnológico de Aeronáutica, CTA, São José dos Campos, BRAZIL
enda.bigarella@gmail.com

João Luiz F. Azevedo
Instituto de Aeronáutica e Espaço, CTA, São José dos Campos, BRAZIL
azevedo@iae.cta.br

Abstract. *Viscous simulations at high Reynolds and Mach numbers for a typical aerospace application are presented. Turbulence is an important feature for these flow regimes. In order to account for the turbulence phenomena, turbulence models within a RANS-solver framework are considered. The simplest model considered is the SST linear eddy-viscosity closure. A nonlinear representation resulting from an explicit algebraic Reynolds-stress model is also considered. A nonlinear Reynolds-stress transport model is also included. These models are used to investigate complex aerodynamic flows over the first Brazilian satellite launcher vehicle at supersonic flight conditions. The effect of the Reynolds number on such supersonic flight conditions is addressed. Simulation results are compared to available wind-tunnel experimental data. In general, acceptable numerical results are obtained.*

Keywords: *CFD, Turbulence modelling, Aerospace flows, Blunt body*

1. INTRODUCTION

Viscous simulations at high Reynolds and Mach numbers are typical for aerospace applications, such as the ones of interest to Instituto de Aeronáutica e Espaço (IAE). Turbulence is certainly an important feature for these flow regimes, and the correct evaluation of the turbulence effects is decisive for consistent computation of complex phenomena such as boundary layers subjected to adverse-pressure gradients, boundary-layer/shock-wave interactions, mixing layers, and others. Such phenomena strongly affect the final aerodynamic result, including even the macro quantities that are usually enough for engineering purposes, such as integrated lift, drag, and moment coefficients.

The present paper reports on a 3-D, unstructured-mesh, finite-volume method that solves the Reynolds-averaged Navier-Stokes (RANS) equations, developed by the CFD group at IAE. In order to account for the missing turbulence effects in the RANS framework, turbulence models are considered. The Menter (1993) SST two-equation, linear, eddy-viscosity model is available. This linear approximation resulting from the Boussinesq hypothesis is further extended to include a nonlinear representation resulting from an explicit algebraic Reynolds-stress model (EARSM) (Wallin and Johansson, 2000). For the utmost modelling effort, the Batten et al. (1999) Reynolds-stress transport model (RSM) is also included. Its formulation naturally offers the potential for more reliable predictions, since important terms are treated exactly. The implementation of such models has been validated using standard test cases from the literature (Bigarella et al., 2004; Bigarella and Azevedo, 2006).

The previously cited models are used to investigate complex aerodynamic flows over the first Brazilian satellite launcher (VLS) vehicle. Supersonic flow conditions about the VLS second-stage flight configuration are considered. For these flows experimental data obtained through numerous wind tunnel tests are available (Moraes Jr. and Augusto Neto, 1990). Numerical results are compared to the experimental data in order to assess the level of agreement of the turbulent flow simulation capability. The effects of the Reynolds number and the Mach number over the turbulence flow field are addressed. In general, good results within engineering error bounds are obtained.

2. THEORETICAL AND NUMERICAL FORMULATIONS

2.1 RANS Equations

The flows of interest in the present context are modelled by the 3-D compressible Reynolds-averaged Navier-Stokes (RANS) equations, written in dimensionless form and assuming a perfect gas, as

$$\frac{\partial \mathbf{Q}}{\partial t} + \nabla \cdot (\mathbf{P}_e - \mathbf{P}_v) = 0 \,, \qquad \mathbf{Q} = \left[\begin{array}{cccc} \rho & \rho u & \rho v & \rho w & e \end{array} \right]^{\mathrm{T}} \,, \tag{1}$$

where $\mathbf{Q}$ is the dimensionless vector of conserved variables, ρ is the fluid density, $\mathbf{v} = \{u, v, w\}$ is the Cartesian velocity vector and e is the fluid total energy per unit of volume. The inviscid flux vector, $\mathbf{P}_e$, and the viscous flux vector, $\mathbf{P}_v$, are

given as

$$\mathbf{P}_e = \left\{ \begin{array}{c} \rho\,\mathbf{v} \\ \rho\,u\mathbf{v} + p\,\hat{\imath}_x \\ \rho\,v\mathbf{v} + p\,\hat{\imath}_y \\ \rho\,w\mathbf{v} + p\,\hat{\imath}_z \\ (e+p)\,\mathbf{v} \end{array} \right\}, \quad \mathbf{P}_v = \frac{1}{Re} \left\{ \begin{array}{c} 0 \\ \left(\tau^{\ell}_{xi} + \tau^{t}_{xi}\right)\,\hat{\imath}_i \\ \left(\tau^{\ell}_{yi} + \tau^{t}_{yi}\right)\,\hat{\imath}_i \\ \left(\tau^{\ell}_{zi} + \tau^{t}_{zi}\right)\,\hat{\imath}_i \\ \beta_i\,\hat{\imath}_i \end{array} \right\}, \tag{2}$$

where Re is the Reynolds number. The shear-stress tensor is defined by

$$\tau^{\ell}_{ij} = \mu_\ell \left[\left(\frac{\partial u_i}{\partial x_j} + \frac{\partial u_j}{\partial x_i} \right) - \frac{2}{3} \frac{\partial u_m}{\partial x_m} \delta_{ij} \right], \tag{3}$$

where u_i is the Cartesian velocity component, and x_i is the Cartesian coordinate. The viscous force work and heat transfer term, β_i, is defined as $\beta_i = \tau_{ij} u_j - q_i$, where the heat transfer component is defined as

$$q_j = -\gamma \left(\frac{\mu_\ell}{Pr} + \frac{\mu_t}{Pr_t} \right) \frac{\partial(e_i)}{\partial x_j}, \tag{4}$$

where e_i is the internal energy; Pr and Pr_t are the laminar and turbulent Prandtl numbers; γ is the ratio of specific heats; and the eddy viscosity coefficient μ_t is discussed in the section to come. It is important to remark here that, for the flow conditions of interest here, the Reynolds analogy for the turbulent heat transfer, as considered in Eq. (4), is adequate and numerically robust. The molecular dynamic viscosity coefficient, μ_ℓ, is computed by the Sutherland law (Anderson, Jr., 1991). The dimensionless pressure, p, can be calculated from the perfect gas equation of state.

This set of equations is solved according to a finite volume formulation. For convective-flux calculations on the volume faces, a Roe (1981) flux-difference splitting scheme is currently used. In order to achieve 2nd-order of accuracy in space, properties are linearly reconstructed in the faces based on the MUSCL (van Leer, 1979) algorithm. The implementation follows a modified and generalised Barth and Jespersen (1989) multidimensional limiter formulation (Bigarella and Azevedo, 2005). The van Albada (Bigarella and Azevedo, 2005) limiter is used to avoid oscillations near discontinuities. Diffusive-flux terms are discretized based on a usual centred scheme, with properties in the faces obtained as an arithmetical average of the properties in the neighbouring cells. Flow equations are integrated in time by a fully explicit, 2nd-order accurate, 5-stage, Runge-Kutta time stepping scheme. An agglomeration full-multigrid scheme (FMG) is included in order to achieve better convergence rates for the simulations. More details on the theoretical and numerical formulations can be found in Bigarella et al. (2004); Bigarella and Azevedo (2006).

2.2 Turbulence Model Equations

The turbulence effects are included into the RANS equations by the Reynolds-stress tensor, defined by

$$\tau^{t}_{ij} = -Re\,\rho\,\overline{u''_i u''_j}\,. \tag{5}$$

Various turbulence models are available in the current code, ranging from linear and nonlinear eddy-viscosity models, to Reynolds stress models. The model transport equations are also solved according to the finite volume approach. The time march is performed using an implicit Euler scheme (Scalabrin, 2002). More details on the numerical scheme for the turbulence transport equations can be found in Bigarella and Azevedo (2006).

3. TURBULENCE MODELS

3.1 Shear-Stress Transport (SST) Model

Eddy viscosity models compute the Reynolds stresses (Eq. 5) through the Boussinesq hypothesis, which states that the turbulence stresses are a linear function of the mean flow straining rate times a modifying constant, μ_t, such as

$$\tau^{t}_{ij} = 2\,\mu_t\,S_{ij} - \frac{2}{3}\rho k\,\delta_{ij}\,, \qquad S_{ij} = \frac{1}{2}\left(\frac{\partial u_i}{\partial x_j} + \frac{\partial u_j}{\partial x_i} \right) - \frac{1}{3}\frac{\partial u_m}{\partial x_m}\delta_{ij}\,, \tag{6}$$

where μ_t is differently defined for each turbulence model.

The linear Menter (1993) SST model is derived from a blend of the original Wilcox (1998) k-ω and the standard k-ϵ (Jones and Launder, 1972) models. It solves reported problems of the k-ω closure regarding freestream value dependency (Menter, 1994) while keeping the better numerical behaviour of this model close to the wall. Model constants are generally calculated as $\phi = F_1\phi_1 + (1 - F_1)\phi_2$, where ϕ_1 represents the set of constants for the k-ω model and ϕ_2, the set for the

standard k-ϵ model, as in Menter (1994). The F_1 variable is a blending function that turns on the k-ω closure near solid walls and the standard k-ϵ model outside boundary layers, and it is dependent on the distance to the wall.

It is known in the CFD community that standard two-equation models are not capable of accurately computing adverse pressure gradients or separated flows (Menter, 1993). These models require a stronger pressure gradient or a longer running length to separate than is indicated by experiments. It is demonstrated that this is a result of the missing effect of turbulent shear-stress transport in this type of flow (Johnson and King, 1985). In order to take the shear-stress into account, at least in an ad-hoc fashion, the eddy viscosity coefficient for the SST model is bounded by a measure of the flow strain rate (Menter, 1994). Another blending function is used to turn on this criterion only inside boundary layers. A careful discussion on the motivations for this procedure can be found in Menter (1993).

A simpler version of the SST model, denoted as the BSL model (Menter, 1993), exactly follows the above formulation, however without the last criterion for the eddy viscosity coefficient. Both BSL and SST models can be integrated to the wall when $y^+ \approx 1$ near the wall.

3.2 Modified Craft-Launder RSM (CLMRSM)

Reynolds stress models use the exact equations for the transport of Reynolds stresses obtained by taking velocity-weighted moments of the Navier-Stokes equations and neglecting density fluctuations. The general form of a RSM is given by

$$\frac{D\rho\overline{u_i'' u_j''}}{Dt} = P_{ij} + D^{\nu}_{ij} + D^{t}_{ij} + D^{p}_{ij} + \Phi^{*}_{ij} - \epsilon_{ij} \,, \tag{7}$$

with the individual terms representing specific turbulence mechanisms, where P_{ij} is the turbulent production; D^{ν}_{ij} is the molecular diffusion; D^{t}_{ij} is the turbulent diffusion; D^{p}_{ij} is the pressure diffusion; Φ^{*}_{ij} is the pressure-strain correlation; and ϵ_{ij} is the turbulent dissipation. The turbulent production and the molecular diffusion terms do not require modelling.

The Batten et al. (1999) RSM is a variation of the Craft and Launder (1996) RSM, which does not require wall-topology parameters such as normal-to-wall vectors and distance from the wall. Modifications of some wall-proximity corrections have been applied to correct the latter model incorrect response to shock waves, which were falsely interpreted as regions of strong inhomogeneity.

The pressure-strain correlation is considered a critical element for RSMs since it can be of the order of the production and dissipation terms, hence playing a crucial role in most flow cases. Instead of a wall-normal vector, which can cause problems for complex geometry applications, two turbulence inhomogeneity indicators based on gradients of the turbulent length scale and Lumley's flatness parameter (Lumley, 1978) are used. A cubic pressure-strain model is here used in conjunction with additional coefficients and those inhomogeneity corrections. This option allows for integration through the viscous sublayer and acts consistently through shock waves, which is an important feature for the flows of interest to IAE.

The generalised gradient diffusion hypothesis (GGDH) of Daly and Harlow (1970) is used for the modelling of the turbulent diffusion. A thin-layer approximation of that term, as in Batten et al. (1999), is used here to avoid numerical instabilities in distorted cells. The pressure diffusion is also considered. It is modelled based on inhomogeneity-indicator vectors and Lumley's stress-flatness parameter.

The dissipation tensor blends isotropic and wall-limiting terms, with an additional term to account for the dip in the shear-stress dissipation rate in the buffer layer. An equation for the homogeneous dissipation rate, ϵ^*, is used to determine ϵ. This equation incorporates a few modifications to better match low-Reynolds number effects near solid walls (Batten et al., 1999).

3.3 Wallin-Johansson EARSM (NLBSL)

The main motivation in the development of EARSMs is the general need for improvements in the prediction of complicated turbulent flow phenomena using the platform of existing CFD codes based on two-equation eddy-viscosity turbulence modelling capability. This is an interesting way of cheaply incorporating advanced turbulence effects, such as streamline curvature and normal stress separation, into an already existing two-equation turbulence model framework, avoiding thus the large amount of computational resources required by the solution of RSMs.

The classical algebraic RSM (ARSM) starts by assuming equilibrium turbulence, which is equivalent to neglecting advection and diffusion for the transport equations of the Reynolds-stress anisotropy tensor. In the formulation of Wallin and Johansson (2000), an isotropic assumption for the dissipation tensor along with a linear pressure-strain correlation are chosen. Substituting those terms into the ARSM, one gets an implicit algebraic equation for the Reynolds-stress anisotropy tensor. The solution of this implicit equation is numerically cumbersome and, thus, a general form for the anisotropy tensor in terms of strain and rotation tensors is proposed (Wallin and Johansson, 2000). This general form for the anisotropy tensor implies the use of initially unknown coefficients.

The explicit solution for the anisotropy tensor now relies on the determination of these coefficients. Some researches

adopt the approach of calibrating those terms to a set of representative turbulence problems (Craft et al., 1996). This approach, however, may decrease the generality of the additional nonlinear Reynolds-stress tensor components. The approach in Wallin and Johansson (2000) substitutes the anisotropy tensor expansion in the implicit ARSM equation. A solution to the unknown expansion coefficients can, thus, be found as detailed in that work. The compressible formulation along with an ad-hoc modification to recast, at least qualitatively, the initially neglected diffusion, as available in Wallin and Johansson (2000), is chosen in the present work.

The EARSM is implemented as a plug-in for the BSL background model. The nonlinear Reynolds stresses are provided by the proposed tensor expansion such as

$$-\rho\overline{u_i'' u_j''} \approx 2\, C_\mu^{eff}\, \frac{\rho k^2}{\epsilon}\, S_{ij} - \frac{2}{3}\rho k\, \delta_{ij} - \rho k\, a_{ij}^{nl}\,. \tag{8}$$

The first two terms in the RHS of the previous equation are similar to those used for linear models, derived from the Boussinesq hypothesis. An effective eddy-viscosity coefficient, C_μ^{eff}, however, is adopted. This coefficient is one of the major contributions of EARSMs because it adapts to the local strain and vorticity fields, which, for instance, removes the need for the strain-rate-based bound in the eddy-viscosity definition of the SST model. The remaining *anisotropic* contribution is wrapped in the a_{ij}^{nl} tensor (Wallin and Johansson, 2000). The nonlinear representation of the current EARSM is implemented over the recalibrated BSL model framework as in Hellsten (2004, 2005).

4. RESULTS AND DISCUSSION

4.0.1 VLS at $M_\infty = 1.25$ and $\alpha = 4$ deg.

The turbulent flow with freestream Mach number $M_\infty = 1.25$ and angle of attack $\alpha = 4$ deg. about the VLS second stage flight configuration is considered. Similarly to the available wind-tunnel experimental results, the Reynolds number per unit length is $Re = 22.4 \times 10^6\, m^{-1}$. Because there are not enough information on the wind-tunnel conditions, the freestream turbulence intensity level is assumed to be 0.5%. This value is considered to be representative of the higher intensities usually found in wind-tunnel flows. The mesh is built with $196 \times 85 \times 36$ hexahedral cells in the longitudinal, wall-normal, and azimuthal directions. The mesh is also clustered near the wall to guarantee a good resolution of the boundary layer, with about 40 points within it, and with $y^+ \approx 1$ near the wall.

Mach number contours obtained with the three turbulence models can be found in Fig. 1. All simulations realistically capture the position of the detached shock wave near the vehicle nose, as well as the expansion waves in the convex corners of the geometry. An adverse pressure gradient associated with a shock wave in the boattail-cylinder junction can also be found.

In Fig. 2, numerical pressure coefficient, Cp, distributions over the VLS wall at the pitching plane are compared to the available experimental data. As one can see in this figure, all turbulence models have similar and good behaviour in predicting the correct trends in the Cp distribution when compared to the experimental data. This positive behaviour also includes the consistent prediction of the complex boundary layer/shock wave interaction in the compression corner at the vehicle boattail-cylinder junction, represented by a slow recompression in the Cp in Fig. 2.

4.0.2 VLS at $M_\infty = 3.00$ and $\alpha = 0$ deg.

A supersonic flow, with $M_\infty = 3.00$ and $\alpha = 0$ deg., about the VLS second-stage flight configuration is now considered. For this flow condition, similarly to the available wind-tunnel experimental results, the Reynolds number per unit length is $Re = 9.3 \times 10^6\, m^{-1}$. This test case is intended to address the sensitivity of the turbulence models to the influence of the Reynolds number. For this flight condition, especially because of the relatively low Reynolds number condition, there is a separated-flow region in the boattail-cylinder junction. For the forthcoming analyses, the three discussed turbulence models are chosen. A laminar flow simulation, that is, without turbulence closure, is also considered.

Numerical Mach number contours for the current simulations are shown in Fig. 3. It is interesting to observe in that figure that all numerical solutions are close to each other, except for the laminar flow solution in which a large separated region in the payload fairing-boattail junction region can be seen. All solutions capture the detached shock wave in the vehicle nose region, as well as the expansion waves in the expansion corners of the geometry. All turbulence-modelled flows present attached boundary layers in the payload fairing-boattail junction region, and subsequently an oblique shock wave stronger than that found in the laminar flow case.

In Fig. 4, numerical Cp distributions over the VLS wall are compared to the respective experimental data. It can be clearly observed in that figure that all turbulence models fail to reproduce the experimentally-obtained separation in the payload fairing-boattail junction region, although other flow trends compare well with the experimental data. Unexpectedly, at least initially, the laminar flow simulation compares strikingly well with the experimental data.

Under detailed analyses this result is a strong indication of a possible relaminarisation phenomenon in the wind tunnel tests which is not captured by the turbulence models. Further analyses in the literature (Arnette et al., 1996; Schneider,

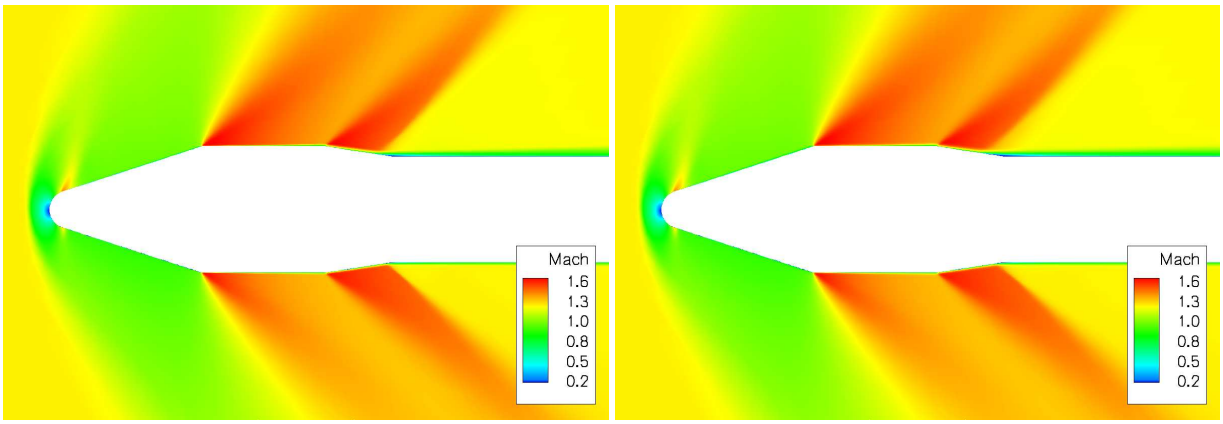

(a) SST.

(b) NLBSL.

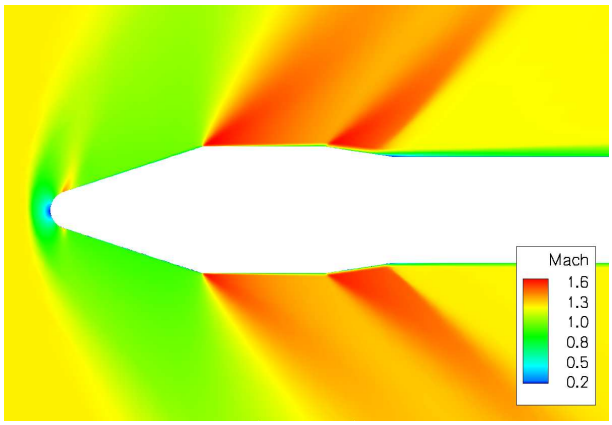

(c) CLMRSM.

Figura 1. Mach number contours over the VLS at $M_\infty = 1.25$ and $\alpha = 4$ deg. for three turbulence models.

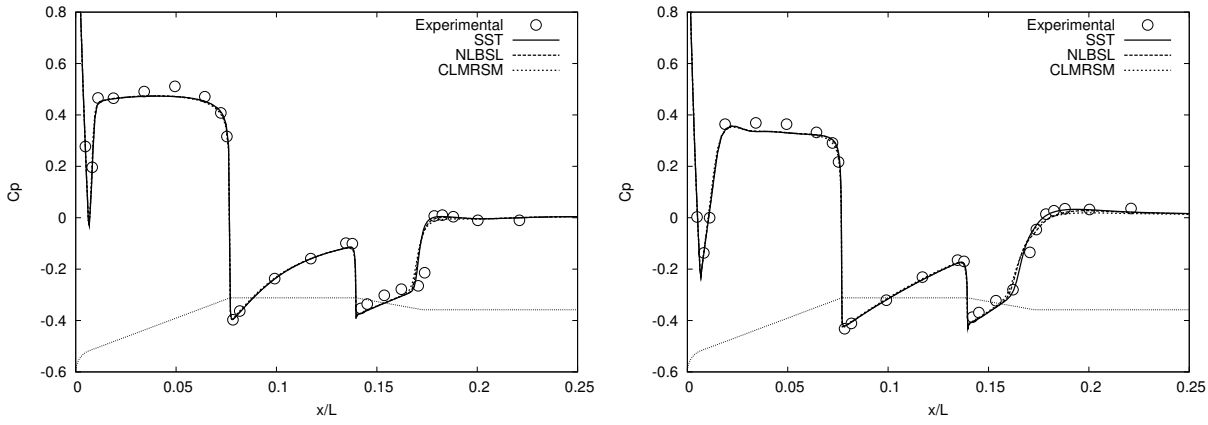

(a) Windside.

(b) Leeside.

Figura 2. Numerical and experimental Cp distributions over the VLS at $M_\infty = 1.25$ and $\alpha = 4$ deg.

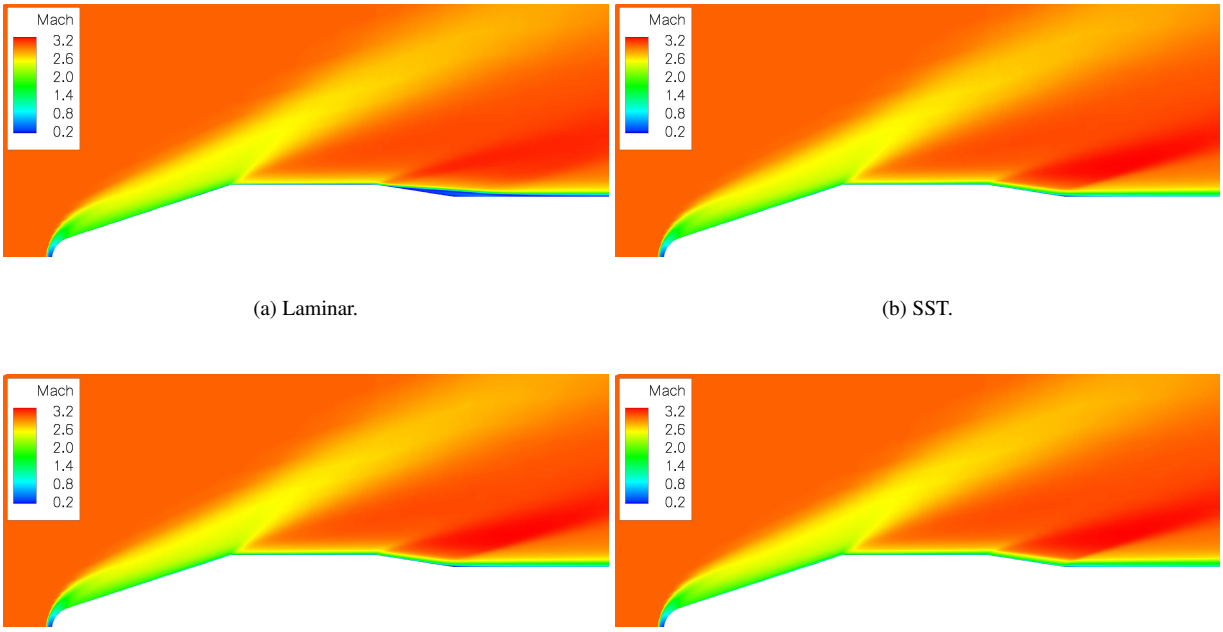

(a) Laminar.

(b) SST.

(c) NLBSL.

(d) CLMRSM.

Figura 3. Mach number contours over the VLS at $M_\infty = 3.00$, $\alpha = 0$ deg., and $Re = 9 \times 10^6\, m^{-1}$.

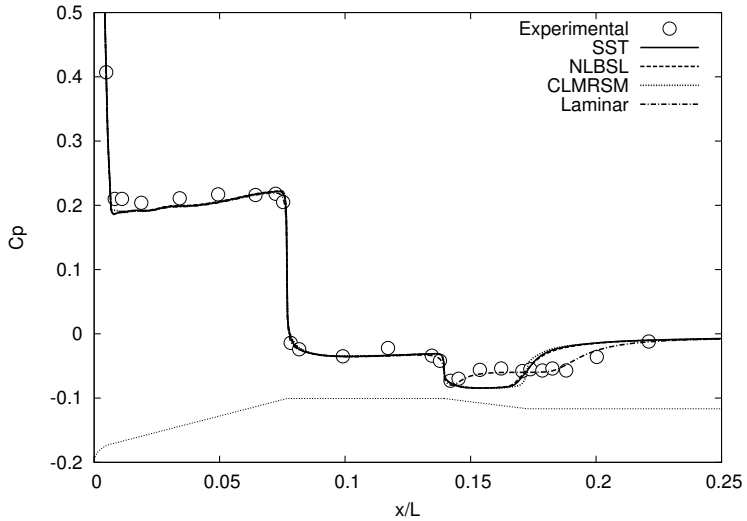

Figura 4. Cp distributions over the VLS at $M_\infty = 3.00$, $\alpha = 0$ deg., and $Re = 9 \times 10^6\, m^{-1}$.

1999; Goldfeld et al., 2002) indicate that such phenomena is typical and usual for supersonic flows. For such flow cases, expansion corners create strongly favourable pressure gradients large enough to promote relaminarisation of the upstream turbulent boundary layer. Lien et al. (1998) brings an acceleration parameter, $K = (\nu/U_e^2)(\partial U_e/\partial x)$, where U_e is the outer irrotational-field velocity. This parameter indicates that relaminarisation occurs for $K > 3 \times 10^{-6}$. Applying this definition to the current VLS flow case, it is found that for the first expansion corner, $K = 10 \times 10^{-6}$, and for the second one, $K = 2 \times 10^{-6}$. These values are a concrete indication of largely favourable relaminarisation conditions for the current VLS flow condition. Wind-tunnel results in Goldfeld et al. (2002) indicate that, even for higher Reynolds number conditions, relaminarisation also occurs.

Further consultation into the literature brings an interesting characteristic of the relaminarised boundary layer, which although not presenting a logarithmic inertial region, it is still kinetically unstable and in a transitional state (Arnette et al., 1996). This unstable, although not turbulent, state may be sustained within large lengths, up to 200 boundary-layer thicknesses, because of the stabilising effect of the flow compressibility, and the absence of considerable velocity gradients in the outer portion of the boundary layer. Therefore, a turbulence model suitable for such complex flow phenomenon should definitely be capable of modelling all the transition-to-turbulence aspects, including even the transition length. This is not the case with the currently chosen turbulence models. The advanced Reynolds-stress CLMRSM closure, in special, although being a low-Reynolds-number turbulence model, is only capable of roughly predicting the transition-to-turbulence point, but not the transition length. Hence, despite all the complexity of the CLMRSM model, one should not actually expect that even this closure would correctly reproduce the current flow-case results.

5. CONCLUDING REMARKS

The paper presents results obtained with a finite volume code developed to solve the compressible RANS equations. Turbulence effects are included by advanced turbulence models, which are specifically designed for aerospace-type flows. The options here range from linear to nonlinear eddy-viscosity models, as well as Reynolds-stress closures. An explicit algebraic expansion of a simplified Reynolds-stress equation is used to compose the nonlinear model.

Supersonic flow simulations about the VLS geometry indicates that the anisotropy of the normal Reynolds-stresses is only marginally better for the current supersonic cases. The NLBSL model, however, presents results which are close to those of the Reynolds-stress model, but at the computational costs of the SST model. This observation represents a good cost-effect compromise for this turbulence model.

All models fail to predict the relaminarisation effect due to the strong flow expansion at the convex corners for the higher Mach number flow. In this case, a relatively low Reynolds number along with such strong expansions allow for flow relaminarisation. Current turbulence models can at most predict a transition location, in the case of CLMRSM, but they are not capable of predicting the transition length after the expansion corners.

For a fully turbulent flow case, the turbulence models here considered return very adequate results. In flows in which relaminarisation may occur, the prediction is less accurate. Nevertheless, the models currently implemented in the code and the experience acquired in the present study have advanced the capability of simulating the transonic and supersonic flows of interest to IAE, which motivated the current effort.

6. ACKNOWLEDGEMENTS

The authors would like to acknowledge Conselho Nacional de Desenvolvimento Científico e Tecnológico, CNPq, which partially supported the project under the Integrated Project Research Grants No. 501200/2003-7 and 312064/2006-3. The authors also acknowledge Dr. P. Batten at Metacomp Technologies, USA, and Dr. S. Wallin at Linköping University, Sweden, for their insights on specifics of the respective turbulence model implementations.

Referências

Anderson, Jr., J. D., 1991. *Fundamentals of Aerodynamics*, chapter 15, pp. 647. McGraw-Hill International Editions, New York, NY, USA, second edition.

Arnette, S. A., Samimy, M., & Elliot, G. S., 1996. The effects of expansion regions on the turbulence structure of compresible boundary layers. In *34th AIAA Aerospace Sciences Meeting and Exhibit*, AIAA Paper No. 96-0656, Reno, NV.

Barth, T. J. & Jespersen, D. C., 1989. The design and application of upwind schemes on unstructured meshes. In *27th AIAA Aerospace Sciences Meeting*, AIAA Paper No. 89-0366, Reno, NV.

Batten, P., Craft, T. J., Leschziner, M. A., & Loyau, H., 1999. Reynolds-stress-transport modeling for compressible aerodynamics applications. *AIAA Journal*, vol. 37, n. 7, pp. 785–796.

Bigarella, E. D. V. & Azevedo, J. L. F., 2005. A study of convective flux computation schemes for aerodynamic flows. In *43rd AIAA Aerospace Sciences Meeting and Exhibit*, AIAA Paper No. 2005-0633, Reno, NV.

Bigarella, E. D. V. & Azevedo, J. L. F., 2006. Advanced eddy-viscosity and reynolds-stress turbulence model simulations of aerospace applications. In *24th AIAA Applied Aerodynamics Conference*, AIAA Paper No. 2006-2826, San Francisco, CA.

Bigarella, E. D. V., Basso, E., & Azevedo, J. L. F., 2004. Centered and upwind multigrid turbulent flow simulations with applications to launch vehicles. In *22nd AIAA Applied Aerodynamics Conference and Exhibit*, AIAA Paper No. 2004-5384, Providence, RI.

Craft, T. J. & Launder, B. E., 1996. A Reynolds stress closure for complex geometries. *International Journal of Heat and Fluid Flow*, vol. 17, n. 3, pp. 245–254.

Craft, T. J., Launder, B. E., & Suga, K., 1996. Development and application of a cubic eddy-viscosity model of turbulence. *International Journal of Heat and Fluid Flow*, vol. 17, n. 2, pp. 108–115.

Daly, B. & Harlow, F., 1970. Transport equation in turbulence. *Physics of Fluids*, vol. 13, pp. 2634–2649.

Goldfeld, M. A., Nestoulia, R. V., & Shiplyuk, A. N., 2002. Relaminarization of a turbulent boundary layer with a mach number $m_\infty = 4$. *Journal of Applied Mechanics and Technical Physics*, vol. 43, n. 1, pp. 76–82.

Hellsten, A., 2004. *New Two-Equation Turbulence Model for Aerodynamics Applications*. PhD thesis, Helsinki University of Technology, Laboratory of Aerodynamics, P.O.Box 4400, Finland.

Hellsten, A., 2005. New advanced k-ω turbulence model for high-lift aerodynamics. *AIAA Journal*, vol. 43, n. 9, pp. 1857–1869.

Johnson, D. A. & King, L. S., 1985. A mathematically simple turbulence closure model for attached and separated turbulent boundary layers. *AIAA Journal*, vol. 23, n. 11, pp. 1684–1692.

Jones, W. P. & Launder, B. E., 1972. The prediction of laminarization with a two-equation model of turbulence. *International Journal of Heat and Mass Transfer*, vol. 15, n. 2, pp. 301–314.

Lien, F. S., Kalitzin, G., & Durbin, P. A., 1998. Rans modeling for compressible and transitional flows. In *Proceedings of the 1998 Summer Program*, Center for Turbulence Research, Stanford University, Stanford, CA.

Lumley, J. L., 1978. Computational modeling of turbulent flows. In Yih, C. -S., ed, *Advances in Applied Mechanics*, volume 18, pp. 123–176. Academic Press, New York.

Menter, F. R., 1993. Zonal two equation $k - \omega$ turbulence models for aerodynamic flows. In *24th AIAA Fluid Dynamics Conference*, AIAA Paper No. 93-2906, Orlando, FL.

Menter, F. R., 1994. Two-equation eddy-viscosity turbulence models for engineering applications. *AIAA Journal*, vol. 32, n. 8, pp. 1598–1605.

Moraes Jr., P. & Augusto Neto, A., 1990. Aerodynamic experimental investigation of the brazilian satellite launch vehicle (vls). In *Proceedings of the 3rd Brazilian Thermal Sciences Meeting – ENCIT 90*, volume 1, pp. 211–215, Itapema, SC, Brazil.

Roe, P. L., 1981. Approximate riemann solvers, parameter vectors, and difference schemes. *Journal of Computational Physics*, vol. 43, n. 2, pp. 357–372.

Scalabrin, L. C., 2002. Numerical simulation of three-dimensional flows over aerospace configurations. Master's thesis, Instituto Tecnológico de Aeronáutica, São José dos Campos, SP, Brazil.

Schneider, S. P., 1999. Fligh data for boundary-layer transition at hypersonic and supersonic speeds. *Journal of Spacecraft and Rockets*, vol. 36, n. 1, pp. 8–20.

van Leer, B., 1979. Towards the ultimate conservative difference scheme. v. a second-order sequel to godunov's method. *Journal of Computational Physics*, vol. 32, n. 1, pp. 101–136.

Wallin, S. & Johansson, A. V., 2000. An explicit algebraic Reynolds stress model for incompressible and compressible turbulent flows. *Journal of Fluid Mechanics*, vol. 403, pp. 89–132.

Wilcox, D. C., 1998. *Turbulence Modeling for CFD*. DCW Industries, La Cañada, CA, second edition.